Experimental analysis of nanostructured PEEK, African giant snail shell, and sea snail shell powder for hydroxyapatite formation for bone implant applications

Esoso, Agbor A.; Jen, Tien Chien; Ikumapayi, Omolayo M.; Oladapo, Bankole I.; Akinlabi, Esther T.

DOI:
10.1016/j.jcomc.2023.100398

Publication date:
2023

Composites Part C: Open Access 12 (2023) 100398

Contents lists available at ScienceDirect

Composites Part C: Open Access

journal homepage: www.sciencedirect.com/journal/composites-part-c-open-access

Experimental analysis of nanostructured PEEK, African giant snail shell, and sea snail shell powder for hydroxyapatite formation for bone implant applications

Agbor A. Esoso [a,*], Tien-Chien Jen [a], Omolayo M. Ikumapayi [b], Bankole I. Oladapo [c], Esther T. Akinlabi [d]

[a] Department of Mechanical Engineering Science, University of Johannesburg, Johannesburg 2006, South Africa
[b] Department of Mechanical and Mechatronics Engineering, Afe Babalola University, Ado Ekiti 360101, Nigeria
[c] School of Science and Engineering, University of Dundee, Dundee, UK
[d] Department of Mechanical and Construction Engineering, Northumbria University, Newcastle, UK

ARTICLE INFO

Keywords:
Bone implants
Furrow depth
Hydroxyapatite coatings
Material ratio
Nanostructure analysis
PEEK

ABSTRACT

This experimental research focuses on the nanostructure analysis of three materials; polyether ether ketone (PEEK), African land giant snail shell (ALGSS), and sea snail shell (SSS) powder, for the formation of hydroxyapatite (HA) coatings in bone implant applications. The study aimed to evaluate these materials' surface characteristics, furrow depth, density, and other relevant parameters to assess their suitability as bone implant materials. The nanostructure analysis revealed distinct characteristics for each material. PEEK exhibited shallow furrows and a high density of furrows, making it a favourable substrate for hydroxyapatite coating formation. The ISO 25178 roughness analysis further characterised surface roughness and topography. African land giant snail shell powder, displayed a high material ratio, indicating a potential for hydroxyapatite conversion for biomedical application. The sea snail shell powder demonstrated intermediate furrow depth and density, warranting further investigation for optimisation as a precursor for hydroxyapatite coatings. The findings emphasise the significance of nanostructure properties in bone implant materials. The tailored nanostructure of materials such as PEEK, the synthesized powder can influence their biocompatibility, osseointegration, and long-term performance. The novelty of this research lies in the comprehensive analysis of the nanostructure properties of these materials, contributing to the understanding of their potential for bone implant applications. Overall, this experimental research is significant and provides valuable insights into the nanostructure characteristics of PEEK, African land giant snail shell powder, and sea snail shell powder and they all demonstrated the potential of forming hydroxyapatite coatings. These findings contribute to advancements in bone implantology, paving enhancing innovative and improved bone implant materials

1. Introduction

Bone implants play a critical role in orthopaedic surgery, enabling the restoration of damaged or diseased bone structures and improving the quality of life for patients. Bone implants' success relies heavily on choosing suitable materials [1–3]. Over the years, there has been growing interest in developing nanostructured materials for bone implant applications due to their unique properties, including improved mechanical strength, enhanced biocompatibility, and the ability to mimic the natural structure of bone tissue [4–6]. Hydroxyapatite (HA), a calcium phosphate compound with a chemical formula of $Ca_{10}(PO_4)_6(OH)_2$, is widely regarded as an excellent biomaterial for bone implants. HA exhibits remarkable biocompatibility, bioactivity, and osseoconductivity (is the potential of materials to function as a scaffold that supports bone formation on its surface. In bone implant, it is a very important requirement in bone regeneration response. If scaffold is excluded in the process, new bone has nowhere to form and the implant site may not heal), making it an ideal choice for promoting bone regeneration and integration with the surrounding tissue [7–9]. Recently, there has been a growing interest in utilising nanostructured

* Corresponding author.
E-mail address: esosoaa@abuad.edu.ng (A.A. Esoso).

https://doi.org/10.1016/j.jcomc.2023.100398

Available online 17 September 2023

materials, such as PEEK and various shell powders, as precursors to form hydroxyapatite coatings on implant surfaces. These coatings provide an enhanced bioactive interface, facilitating the integration of the implant with the host bone [10–12].

PEEK, a high-performance polymer, has gained significant attention as a potential material for bone implants due to its exceptional mechanical properties, chemical stability, and biocompatibility. However, the inherent bio-inertness of PEEK limits its ability to bond directly with bone tissue. To overcome this limitation, incorporating hydroxyapatite on the surface of PEEK implants can enhance their osseoconductivity and biocompatibility [13,14]. Therefore, analysing the nanostructure of PEEK is crucial in understanding its surface characteristics and assessing its suitability as a substrate for hydroxyapatite formation. Natural materials, such as shell powders derived from African land giant and sea snail shells, offer an alternative approach to obtaining hydroxyapatite coatings. These shell powders primarily comprise calcium carbonate ($CaCo_3$) and possess a hierarchical structure that resembles that of natural bone [15–17]. Subjecting these shell powders to appropriate processing techniques, including thermal treatment and acid etching, can transform the calcium carbonate structure into hydroxyapatite. The resulting nanostructured hydroxyapatite coatings can significantly enhance the biocompatibility and osseointegration (a medical or clinical term that is used to describe the fusion process in the curing process of an implant) of bone implants [18–20].

The characterisation and analysis of nanostructured materials are critical in determining their surface roughness, furrow depth, density, and other relevant structural parameters. These properties directly influence the material's interaction with the surrounding biological environment, including cell adhesion, proliferation, and tissue integration [21–23]. Various characterisation techniques, such as high-pass robust Gaussian filtering, morphological envelopes, ISO 25178 roughness analysis, and step height calculations, enable a comprehensive understanding of the nanostructure of the materials under investigation. Considering the abovementioned considerations, this experimental research aims to analyse the nanostructure properties of PEEK, African land giant snail shell powder, and sea snail shell powder to assess their potential for forming hydroxyapatite coatings in bone implant applications. The investigation will provide valuable insights into the suitability of these materials for bone implant fabrication, aiding in developing novel and improved hydroxyapatite-based implants.

The research objective of this paper, is to conduct a nanostructure analysis of three materials (PEEK, African giant snail shell powder, and sea snail shell powder) for their potential use in forming hydroxyapatite coatings for bone implant applications. The study aims to evaluate the surface characteristics, furrow depth, density, and other relevant parameters of these materials to assess their suitability as bone implant materials. The Specific Materials Being Studied in this work are; Polyether Ether Ketone (PEEK), African land giant snail shell (ALGSS) Powder and material and, Sea Snail Shell (SSS) Powder. These materials are being studied for its surface characteristics, furrow depth, and, density to determine its suitability as a substrate for hydroxyapatite coating formation in bone implants. This work is significant to providing valuable insights into the potential of these materials as bone implant materials for forming hydroxyapatite coatings, contributing to advancements in bone implantology and paving the way for innovative and improved materials with enhanced biocompatibility and clinical outcomes.

2. Literature review

Developing bone implant materials with enhanced biocompatibility and osteoconductive has been a focus of extensive research in orthopaedics. Nanostructured materials, such as PEEK, natural biomaterials, and their derivatives, have gained significant attention due to their unique properties and potential for promoting bone regeneration [24–26]. This literature review aims to provide an overview of the existing research and knowledge related to the nanostructure analysis of PEEK, African land giant snail shell powder, and sea snail shell powder to form hydroxyapatite coatings in bone implant applications. PEEK, a high-performance polymer, has emerged as a promising material for bone implants due to its excellent mechanical properties and biocompatibility [27–29]. The nanostructure analysis of PEEK surfaces plays a crucial role in understanding its topographical characteristics, which directly influence cell adhesion, proliferation, and differentiation. Previous studies have shown that the nanostructured surface of PEEK promotes improved osteoblast response and osseointegration. Additionally, incorporating hydroxyapatite coatings on PEEK surfaces can further enhance its bioactivity and bone integration capabilities [30–32].

Natural biomaterials, such as those derived from African land giant and sea snail shells, have attracted interest due to their inherent biocompatibility and potential for hydroxyapatite conversion. The nanostructure analysis of these materials provides insights into their surface roughness, furrow depth, and density, which are critical factors for hydroxyapatite coating formation. African land giant snail shell powder's hierarchical structure and composition offer opportunities to develop biomimetic materials that closely mimic the natural bone environment [33–35]. Similarly, sea snail shell powder presents an intriguing nanostructure for bone implant applications, with the potential for optimisation to enhance its surface properties and promote osteogenic responses. Nanostructured materials for bone implants continue to evolve, with researchers exploring innovative fabrication techniques, surface modifications, and coating strategies to further enhance their biocompatibility and performance. Advanced characterisation techniques, such as ISO 25178 roughness analysis and fractal dimension analysis, allow for a comprehensive understanding of these materials' nanostructure and surface properties [36–38].

In conclusion, the literature reviewed demonstrates the significance of nanostructure analysis in evaluating the potential of materials for bone implant applications. The nanostructure characteristics of PEEK, giant snail shell powder, and sea snail shell powder play crucial roles in their biocompatibility, osseointegration, and overall performance. Further research is warranted to optimise these materials and develop effective strategies for forming hydroxyapatite coatings, ultimately advancing the field of bone implantology and improving patient outcomes in orthopaedic surgery (Table 1).

2.1. Software applications for relevant analysis

The software used for all the analyses on this work is known as MountainsMap, a software suite developed by Digital Surf for surface analysis and metrology. It is commonly used in scientific and industrial applications to analyze surface topography, profile measurements, and

Table 1
Nanostructure analysis of PEEK.

Parameters	Value	Unit
Maximum depth of furrows	0.5527	μm
Mean depth of furrows	0.1342	μm
Mean density of furrows	4.582	cm/cm^2
Fractal dimension	2.644	–
ISO 25178 - Roughness (S-L)		
Root-mean-square height (Sq)	–	nm
Core height (Sk)	27.98	nm
Reduced peak height (Spk)	39.27	nm
Reduced pit depth (Svk)	39.46	nm
Upper bearing area (Smrk1)	15.52	%
lower bearing area (Smrk1)	84.13	%
Plateau root-mean-square deviation (Spq)	*****	–
Dale root-mean-square deviation (Svq)	*****	–
Plateau-to-dale material ratio (Smq)	*****	–
Step height calculations		
Projected area	274.5	mm^2
Mean thickness of the void	1.26×10^{-3}	μm
Mean thickness of the material	0.2487	μm

other related data. It provides tools for visualization, analysis, and reporting of surface texture and morphology. Some of the key features which makes this tool powerful and unique includes; the software allows users to visualize and manipulate 2D and 3D surface data. It provides tools for rendering and displaying surface images, profiles, and maps. Also, MountainsMap offers a wide range of analysis tools for characterizing surface parameters, roughness, texture, wear, and other surface features. Its Filters and Segmentation features includes filtering and segmentation capabilities to preprocess data, remove noise, and focus on specific regions of interest. The software also supports advanced analysis techniques like fractal analysis, statistical analysis, and feature extraction. MountainsMap facilitates the creation of detailed reports and presentations with customizable templates for sharing analysis results. Another significant feature is its Instrument Compatibility, which permits interface with various metrology instruments, such as profilometers, optical profilers, confocal microscopes, and atomic force microscopes (AFMs), this enhances flexibility for multiformat data input. Another key feature is Automation, The software often includes scripting or automation capabilities to streamline repetitive analysis tasks. It may be important to note that software features and versions may evolve over time, so there may have been updates or changes to MountainsMap features since this paper was published. To get updated information about the software's capabilities, current version, or any recent developments, visiting the official website of Digital Surf or directly contacting their support team may be recommended. This software was specifically used for the analysis introduced in the next section of this chapter (Table 2).

2.2. High-pass robust Gaussian filtering

High-pass robust Gaussian filtering is a specific type of image filtering technique used in image processing and computer vision. It combines Gaussian filtering, which smooths the image, with high-pass filtering, which enhances edges and details of the image. The objective of this filtering approach was to reduce noise and other low-frequency components while preserving and enhancing high-frequency details in the image [39,40].

2.2.1. Relevant parameters used for high-pass robust Gaussian filtering analysis

High-pass robust Gaussian filtering is commonly used in various image processing tasks, including image enhancement, edge detection, and feature extraction. The specific implementation and parameters for this filtering technique may vary depending on the application and the characteristics of the images being processed. The processes and relevant parameters used for high-pass robust Gaussian filtering analysis in this work are explained as follows: Gaussian filtering is a widely used smoothing technique that applies a Gaussian kernel to the image. The Gaussian kernel is a 2D function that emphasizes the central pixel while decreasing the influence of surrounding pixels based on their distance from the center. This smoothing operation was used to effectively reduce noise and blurs the images. High-pass filtering method was used to enhance high-frequency components in the image, such as edges and fine details. It was achieved by subtracting the smoothed version of the image (which obtained from the Gaussian filtering step) from the original image. The resulting images produced contain primarily high-frequency components. However, robust method was used to handle outliers from our resultant images. This filtering technique is less sensitive to outliers or extreme values in the image [41,42]. In the context of high-pass robust Gaussian filtering, the method is designed to handle noisy or corrupted images more effectively. The combination of Gaussian filtering and high-pass filtering in this approach is intended to allow for noise reduction while preserving important image features. The Gaussian filtering step will smoothen the image and reduces noise, while the high-pass filtering step will enhance edges and fine details, making them more prominent (Table 3).

Table 2
Nanostructure analysis of African land giant snail shell powder.

Parameters	Value	Unit
Maximum depth of furrows	84.69	nm
Mean depth of furrows	24.71	nm
Mean density of furrows	3.816	cm/cm^2
Fractal dimension	2.376	–
ISO 25178 - Roughness (S-L)		
Sq	18.55	nm
Sk	51.67	nm
Spk	7.170	nm
Svk	23.39	nm
Smrk1	8.573	%
Smrk2	91.57	%
Sak1	3.07×10^{11}	nm^3/mm^2
Sak2	9.86×10^{11}	nm^3/mm^2
Vmp	4.46×10^{11}	mm^3/mm^2
Vmc	1.80×10^{-5}	mm^3/mm^2
Vvc	2.28×10^{-5}	mm^3/mm^2
Vvv	2.23×10^{-6}	mm^3/mm^2

2.3. Morphological envelope analysis

Morphological envelope analysis is a specific image processing technique used to extract the envelope of a surface profile or image. It involves applying morphological operations to obtain the upper and lower boundaries that envelop the surface profile, capturing its overall shape and characteristics such as furrow height and depth [43].

2.3.1. Parameters used for morphological envelope analysis

Morphological envelope analysis is a technique used in image processing and computer vision to extract the overall shape and characteristics of a surface profile while removing noise and minor irregularities. The process involves several steps that contribute to this analysis. The process begins with an input image representing a surface profile in a 2D format. A structuring element is defined, often taking the form of a small shape like a line or rectangle, which acts as a probe to analyze the image. Two essential morphological operations, erosion and dilation, are then applied to the image using the structuring element. Erosion removes outer points and boundaries, reducing the image's size and smoothing irregularities. Dilation, on the other hand, adds points to enhance features and increase the image size. The morphological envelope is extracted by combining erosion and dilation. The image is eroded to create a smoothed version, and then the dilated version is subtracted. This process reveals the envelope of the original image, capturing its general shape and traits. Morphological envelope analysis

Table 3
Nanostructure analysis of sea snail shell powder.

Parameters	Value	Unit
Maximum depth of furrows	67.75	nm
Mean depth of furrows	7.185	nm
Mean density of furrows	3.816	cm/cm^2
Fractal dimension	2.376	–
ISO 25178 - Roughness (S-L)		
Root-mean-square height (Sq)	19.12	nm
Core height (Sk)	3.587	nm
Reduced peak height (Spk)	2.664	nm
Reduced pit depth (Svk)	3.270	nm
Upper bearing area (Smrk1)	13.24	%
Lower bearing area (Smrk2)	85.73	%
Plateau root-mean-square deviation (Spq)	1.718	–
Dale root-mean-square deviation (Svq)	11.49	–
Plateau-to-dale material ratio (Smq)	98.17	–
Peak material volume (Vmp)	4.46×10^{-7}	mm^3/mm^2
Core material volume (Vmc)	1.80×10^{-5}	mm^3/mm^2
Core void volume (Vvc)	2.28×10^{-5}	mm^3/mm^2
Pit void volume (Vvv)	2.23×10^{-6}	mm^3/mm^2

is valuable in image processing and computer vision, particularly when understanding the overall shape and structure of objects is crucial. It helps filter out noise and complexities, making it a powerful tool for various applications [44,45].

2.4. ISO 25178 roughness analysis

ISO 25178 is a standard developed by the International Organization for Standardization (ISO) titled "Geometrical Product Specifications (GPS) - Surface texture: Areal." This standard provides guidelines and methods for the measurement and characterization of surface texture in three dimensions, specifically for areal (3D) surface texture parameters. ISO 25178 is an essential standard for industries where surface quality is critical, such as automotive, aerospace, medical, and semiconductor manufacturing. It ensures that surface texture measurements are standardized and comparable across different manufacturers and laboratories. To perform ISO 25178 roughness analysis, specialized software and instruments are often used to measure and analyze 3D surface data obtained from techniques like profilometry, confocal microscopy, or atomic force microscopy (AFM). These software tools can automatically calculate the ISO 25178 parameters from the acquired surface data, providing valuable insights into the surface quality and performance of engineering components [46,47].

2.4.1. Relevant parameters used for ISO 25178 roughness analysis

ISO 25178 defines a set of parameters and analysis techniques to quantitatively describe the surface roughness, waviness, and primary profile of engineering surfaces. It is applicable to various surfaces, including those produced by machining, grinding, polishing, and additive manufacturing processes. The ISO 25178 standard covers a wide range of parameters, the ones covered in this work includes:

I Sa (Arithmetic Mean Height): The arithmetic mean of the absolute values of the surface heights from the mean plane.
II Sq (Root Mean Square Height): The root mean square of the surface heights from the mean plane.
III Sz (Maximum Height): The maximum height from the mean plane to the highest peak or deepest valley on the surface.
IV Ssk (Skewness): A measure of the asymmetry of the height distribution.
V Svk (Kurtosis): A measure of the "peakedness" or "flatness" of the height distribution.
VI Sdr (Developed Interfacial Area Ratio): The ratio of the actual surface area to the projected area.
VII Spd (Density of Summit Points): The density of surface points representing summits.
VIII Svi (Voids Index): A measure of the density of voids or pits on the surface.

The ISO 25178 standard specifies methods for filtering, segmentation, and analysis of the surface data to calculate these parameters accurately and consistently. It also defines the procedures for data acquisition, data evaluation, and reporting of results [48–50]. The MountainsMap software deployed in this work, carries high capability to calculate these parameters accurately.

2.5. Step height calculations

Step height calculations are measurements used to quantify the height difference between two distinct regions on a surface or an object. The steps can be defined as changes in height that occur abruptly, often forming distinct edges or discontinuities on the surface. Step height calculations are commonly used in various applications, including surface characterization, quality control, and device fabrication.

The specific algorithms and methods used for step height calculations may vary based on the instrument and software used for data acquisition and analysis. While others may require manual measurements or custom algorithms, some instruments and software packages may provide built-in functions or tools for automated step height measurements, an example of such software is python OpenCV and MountainMap, a software which was utilized in the experiments in this work. Step height calculations are valuable in various industries, such as semiconductor manufacturing, MEMS (Micro-Electro-Mechanical Systems) fabrication, and surface metrology [51]. They play a crucial role in quality control, process optimization, and the characterization of surface features.

2.5.1. Parameters and settings deployed for step height calculations

The determination of relevant parameters and settings for step height calculations is contingent upon the particular measurement technique and instrument employed. In this study, meticulous consideration was given to deploy the following parameters and settings within the Mountain Due software, ensuring precise and accurate step height calculations. Primarily, the data acquisition settings established the foundation for accurate calculations. The sampling rate, a pivotal parameter for techniques like profilometry or AFM, dictated the density of data points acquired, significantly impacting the fidelity of the scan lines or surface measurements. The scan area, indicative of the size of the scanned or measured region, played a vital role in determining the resolution and accuracy of step height calculations. Additionally, the scan range, indicative of the instrument's capacity to measure heights or depths, influenced the upper limit of step height that could be reliably captured. Prior to engaging in step height calculations, data preprocessing procedures were meticulously executed. Flattening or leveling procedures were conducted to eliminate tilt or curvature from the surface data, establishing an essential reference plane.

Furthermore, depending on the data's inherent noise level, appropriate filtering techniques were applied to enhance the signal-to-noise ratio, ensuring cleaner and more accurate measurements. Step detection procedures played a crucial role in isolating significant height changes. Thresholding, implemented through a predetermined threshold value, effectively discriminated between substantial height transitions and incidental noise or fluctuations. Furthermore, the consideration of step width, or the lateral extent of a step, contributed to precise localization of step edges, enhancing the overall accuracy of calculations. The selection of a suitable reference plane emerged as a pivotal determinant. The option to opt for either a fixed reference plane or an adaptive one, varying with the local height distribution, held implications for the accuracy of step height calculations. Subsequently, the step height measurement itself was meticulously managed. The choice between peak height and valley depth measurements, whether peak-to-peak or peak-to-valley, aligned with the intended application and provided consistency in the calculations. To enhance reliability, data averaging played a role through the incorporation of multiple measurement points. By averaging measurements taken at various locations along the step, the precision of step height calculations was bolstered. It is imperative to consult the user manual or relevant documentation of the specific instrument or software convenient to the researcher that may be employed for step height measurements. However, the software tool deployed in this analysis, is the MountainMap software. Comprehensive understanding of available parameters and settings, coupled with their implications on outcomes, remains pivotal. The appropriate calibration and optimization of these parameters stand as foundational elements in achieving accurate and replicable step height calculations, ultimately contributing to the precision of experimental results [52,53].

2.6. Fractal dimension analysis

Fractal dimension analysis is a mathematical technique used to quantify the complexity and self-similarity of fractal-like structures or patterns. Fractals are complex geometric shapes that exhibit self-

similarity at different scales, meaning that the pattern looks similar when zoomed in or out. Fractal dimension is a measure of how a fractal pattern fills space or extends in a multi-dimensional space. In the context of image processing and analysis, fractal dimension analysis is used to characterize the irregularity, roughness, or complexity of objects or patterns. It is particularly valuable for describing complex natural phenomena, such as coastlines, clouds, mountain ranges, and biological structures. Fractal dimension analysis is a mathematical technique used to quantify the complexity and self-similarity of fractal-like structures or patterns. The calculation of fractal dimension involves several methods, and the selection of a specific method is contingent upon the type of data being analyzed and the intrinsic characteristics of the fractal under investigation.

A prevalent approach in fractal dimension analysis is the Box-counting Method. This technique, renowned for its simplicity and widespread utilization, is primarily employed for determining the fractal dimension of two-dimensional patterns. The process entails dividing the pattern into a grid composed of boxes of varying sizes. Subsequently, the number of boxes containing a portion of the pattern is counted, and a plot is generated by juxtaposing the box size against the corresponding count. By examining the slope of the log-log plot, the fractal dimension can be derived. This method serves as a fundamental tool for assessing the complexity of patterns and structures. Expanding the ambit of fractal dimension analysis to encompass more intricate spaces such as curves or three-dimensional structures, the Hausdorff–Besicovitch Method comes into play. This method introduces the concept of "Hausdorff measure," facilitating the quantification of the size or "length" of a fractal across varying scales. By adopting this approach, a broader range of fractals can be characterized, accommodating diverse geometries and configurations [54,55]. The Information Dimension, on the other hand, introduces a distinct perspective to fractal dimension analysis. It evaluates the rate of information expansion relative to resolution, providing a means to quantify the intricacy inherent in fractals. This method offers insights into how the complexity of a fractal evolves as its resolution is refined, shedding light on its self-similar nature. When confronted with three-dimensional structures or volumetric data, the Minkowski–Bouligand Dimension, also referred to as the Box-counting Dimension for 3D, assumes significance. This extension of the box-counting method caters to the analysis of volumetric data, such as three-dimensional rendered images or point clouds. By employing this method, the fractal dimension of complex three-dimensional structures can be ascertained, particularly when capturing the overall shape and structure of objects is of paramount importance. Fractal dimension analysis finds applications in various fields, including image processing, terrain analysis, texture analysis, and pattern recognition. It helps in understanding and quantifying the intricate and self-similar nature of complex natural and artificial structures. The calculated fractal dimension provides valuable insights into the shape, roughness, and overall complexity of the objects being analyzed.

2.6.1. Relevant parameters used for fractal dimension analysis

Fractal dimension analysis serves as a fundamental technique for quantifying the intricacies of fractal-like structures and patterns. Its significance spans various domains, from image processing to terrain analysis, offering insights into the complexity and self-similarity of objects at different scales. The selection of parameters and settings for conducting fractal dimension analysis is a critical determinant of the accuracy and relevance of the results obtained. The specific methodology employed and the characteristics of the data under examination play pivotal roles in guiding these choices. One common method for fractal dimension analysis is the Box-Counting Method, which involves dividing a pattern into boxes and assessing parameters related to this division. The grid size, or the dimensions of these boxes, serves as a crucial parameter. Smaller grid sizes yield more precise outcomes but necessitate heightened computational resources. Moreover, the grid resolution, encompassing the number of divisions along each axis of the grid, influences the level of detail that can be captured in the analysis. In addition to grid-related parameters, data pre-processing is often a prerequisite. This step, involving actions like image thresholding or noise reduction, enhances analysis accuracy by rectifying data irregularities. For the Hausdorff–Besicovitch Method, an iterative algorithm, two critical parameters are considered. The maximum iterations parameter determines the number of iterations performed, impacting the precision of the fractal dimension calculation. Additionally, the convergence criteria, denoting the conditions under which the iterative process halts, significantly influences the outcome of the analysis. When dealing with volumetric data, the Minkowski–Bouligand Dimension (commonly used as the Box-Counting Dimension for 3D structures) necessitates parameters associated with voxel-based analysis. The voxel size, akin to the dimensions of 3D pixels, influences the partitioning of the volume into boxes. Complementing this is the voxel resolution, signifying the number of divisions along each axis of the voxel grid. The choice of these parameters directly affects the granularity of the analysis in three-dimensional space [56,57].

Another avenue of fractal dimension analysis is the Information Dimension, where parameters are linked to the resolution range. This parameter encapsulates the scale over which the information dimension is calculated, directly impacting the scope and accuracy of the analysis outcomes. Data preparation forms a crucial facet of the analysis process. Ensuring consistent units and resolution often involves scaling the data to a standardized format before initiating the analysis. Statistical considerations, including data averaging, play a pivotal role in bolstering the reliability of results. Multiple measurements or analyses of distinct regions may be averaged to mitigate anomalies and enhance the overall accuracy of the analysis. Lastly, in some scenarios, employing smoothing or filtering techniques may be deemed necessary. These techniques are employed to reduce noise or variations in the data, refining the analysis outcomes by accentuating relevant patterns and diminishing extraneous noise. However, the choice of parameters and settings can significantly impact the accuracy and reliability of fractal dimension analysis results. It is essential to carefully select appropriate parameters based on the characteristics of the data and the objectives of the analysis. Additionally, in some cases, the fractal dimension analysis may involve testing different parameter values to assess their impact on the results and select the most suitable settings for the specific application.

3. Methods

3.1. Sample preparation

PEEK high-quality samples were obtained from reliable sources. The samples were carefully cleaned and sterilised using appropriate methods to remove contaminants. African land giant snail shell powder is from African land giant snail shells that were collected, thoroughly cleaned, and dried. The shells were then crushed and ground into a fine powder using a ball milling machine. Shells from sea snails were collected, cleaned, and dried. The shells were processed similarly to the giant snail shells to obtain a fine powder. The sample preparation process is crucial in ensuring accurate and reliable nanostructure analysis of materials for bone implant applications. Proper sample preparation techniques are essential for obtaining representative samples with preserved nanostructure characteristics. This section discusses the sample preparation methods employed for PEEK, giant snail shell powder, and sea snail shell powder in the experimental research [58–60].

The first step in preparing the PEEK samples involved obtaining pristine PEEK specimens. These specimens were carefully cleaned to remove any contaminants or debris that could affect the subsequent analysis. Standard cleaning techniques included ultrasonic cleaning in solvents such as isopropyl alcohol or acetone, followed by air drying or vacuum drying to ensure the complete removal of any residual solvent [61–63]. African land giant snail shell powder and sea snail, shell powder samples required additional preparation steps due to their

natural origin. The shells were collected, thoroughly cleaned to remove any organic matter, and then crushed into a fine powder using a milling machine. The resulting powder was sieved to obtain a uniform particle size distribution, ensuring consistent analysis across the sample. Any oversized particles were discarded, and only the fine powder fraction as depicted in Fig. 1 was used for further research [64–66].

Following the cleaning and preparation of the samples, proper handling and storage procedures were employed to minimise any potential contamination or alteration of the nanostructure. The samples were stored in a controlled environment, protected from light, moisture, and excessive temperature fluctuations. During the sample preparation process, it is crucial to maintain the integrity of the nanostructure and avoid introducing artefacts or changes that could impact the subsequent analysis. Careful attention was given to avoid excessive mechanical stress, temperature variations, or exposure to chemicals that could alter the surface properties or nanostructure of the materials. It is worth noting that the sample preparation methods may vary depending on the analysis techniques' specific requirements. In this research, the samples were prepared to ensure representative and consistent characterisation of the nanostructure properties of PEEK, African land giant snail shell powder, and sea snail shell powder.

Proper sample preparation is crucial for obtaining reliable and accurate nanostructure analysis results. By employing standardised and meticulous sample preparation techniques, the researchers ensured that the received data reflected the nanostructure characteristics of the materials under investigation. This attention to sample preparation enhances the validity and reliability of the experimental findings and facilitates meaningful comparisons and interpretations across different materials and studies. Overall, the sample preparation process is critical in nanostructure analysis, ensuring that the materials' surface characteristics and nanostructure are preserved and accurately represented as depicted in Fig. 2. By following rigorous sample preparation protocols, the researchers obtained suitable samples for the subsequent analysis, enabling a comprehensive evaluation of the materials' nanostructure and their potential for hydroxyapatite coating formation in bone implant applications.

3.2. Nanostructure analysis

High-pass robust Gaussian filtering is the surface profiles of the PEEK samples; African land giant snail shell powder and sea snail shell powder were subjected to high-pass vital Gaussian filtering using specialised software known as Mountain Map. This filtering technique helps remove noise and isolate the relevant nanostructure features. Morphological envelopes are the filtered surface profiles analysed using morphological envelope analysis. This analysis allows for determining essential parameters such as maximum depth of furrows, mean depth of furrows, and mean density of furrows. The threshold values were set to selectively analyse furrows deeper than a specified threshold. ISO 25178 roughness analysis is the filtered surface profiles were further analysed according to ISO 25178 standards. This analysis provides detailed roughness parameters (as seen in Table 1), including Sq, Sku, Spk, Svk, Smrk1, Smrk2, Spq, Svq, and Smq. These parameters offer valuable insights into the surface roughness and topography of the materials. Step height calculations were performed to determine the projected area, mean thickness of the void, and mean thickness of the material. This analysis involved identifying the regions of interest and measuring the height differences between adjacent peaks and valleys. Fractal dimension analysis a fractal dimension analysis was carried out to quantify the complexity of the nanostructures. This involved examining the scaling properties of the surface profiles and determining the fractal dimensions using appropriate algorithms. Fig. 3 shows the weighing of each sample while nanostructure analysis of PEEK is presented in Table 1.

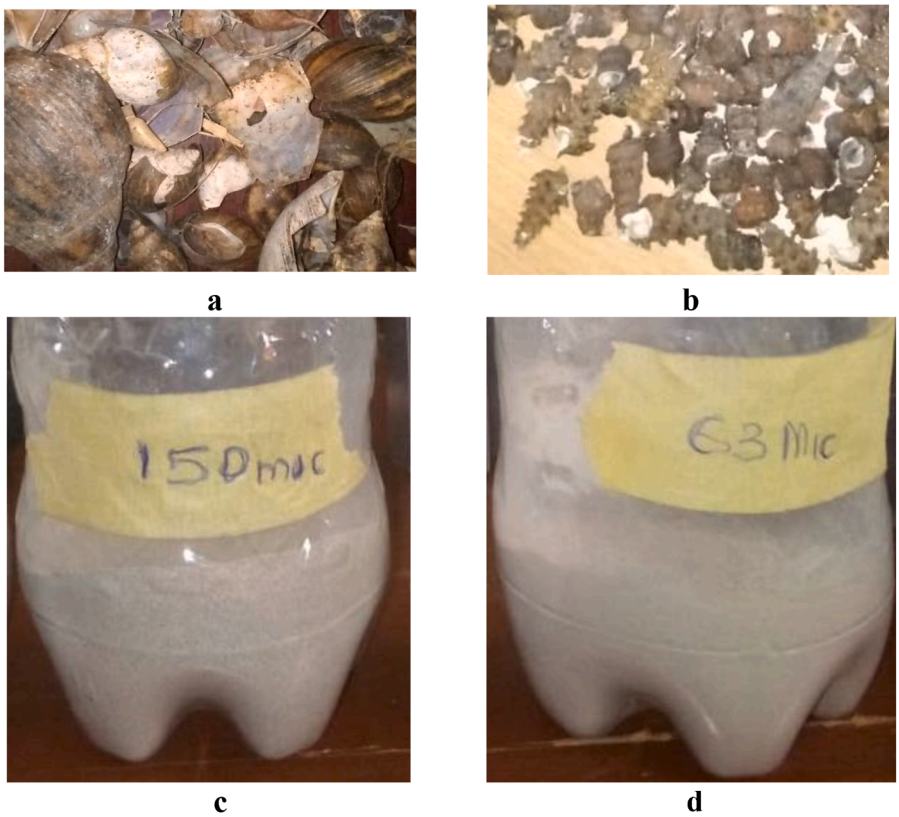

Fig. 1. (a) Giant snail Shell (b) Sea snail shel prepared for acidifying; grinded and treatment at (c) 150 μm (d) 63μm.

Fig. 2. Model SXL maple furnace for preparation of African land giant and sea snail shell.

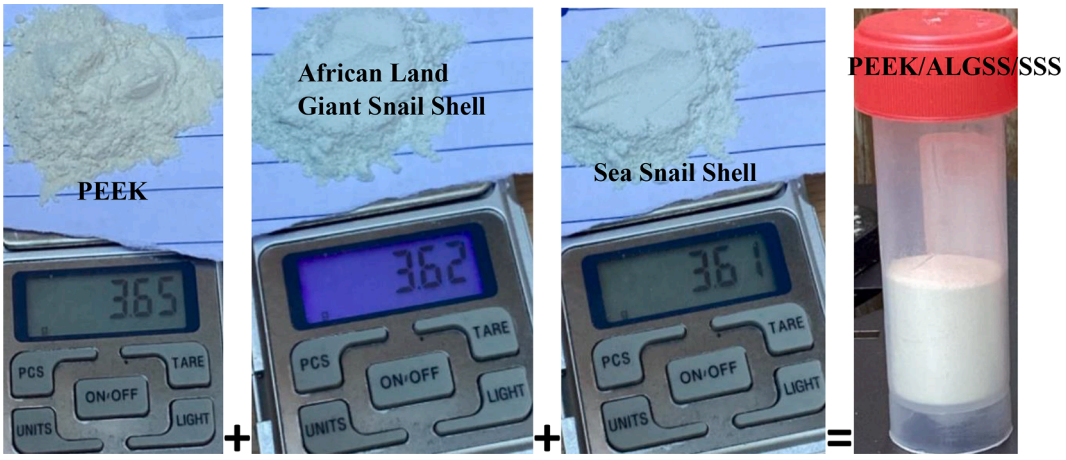

Fig. 3. The composite preparation with PEEK, African land giant snail shell and sea snail shell powder.

3.3. Statistical analysis

The obtained data from the nanostructure analysis were subjected to statistical analysis. Descriptive statistics such as means, standard deviations, and confidence intervals were calculated to summarise the data and evaluate the variations within the samples. Comparative studies, such as t-tests or Analysis of Variance (ANOVA), were conducted to determine significant differences between the materials and identify the key factors influencing the nanostructure properties. Correlation analysis was performed to investigate the relationships between different nanostructure parameters and identify potential trends or associations Table 2 illustrates nanostructure analysis of African land giant snail shell powder while Table 3 shows Sea Snail Shell Powder analysis.

3.4. Limitations

It is essential to acknowledge the limitations of the experimental methods used. Factors such as sample preparation techniques, measurement errors, and the sensitivity of the analysis techniques may introduce some degree of variability and uncertainty in the results. Additionally, the specific characteristics and quality of the PEEK samples, African land giant snail shell powder, and the sea snail shell powder used in the study can influence the outcomes. Therefore, caution must be exercised in generalising the findings to other samples or populations. Overall, the experimental methods employed in this study provide a comprehensive analysis of the nanostructure properties of PEEK, African land giant snail shell powder, and sea snail shell powder. These methods enable a thorough evaluation of the surface characteristics, furrow depth, density, and other relevant parameters, contributing to a deeper understanding of the material's suitability for forming hydroxyapatite coatings in bone implant applications.

4. Results

PEEK exhibited a maximum furrow depth of 0.5527 μm, a mean depth of 0.1342 μm, and a mean density of 4.582 cm/cm^2. The African land giant snail shell powder displayed a maximum furrow depth of 84.69 nm, a mean depth of 24.71 nm, and a mean density of 3.816 cm/cm^2. While the sea snail shell powder showed a maximum furrow depth of 67.75 nm, a mean depth of 7.185 nm, and a mean density of 3.816 cm/cm^2. Various other parameters, such as the fractal dimension, step height calculations, and ISO 25178 parameters, were obtained for each material. The nanostructure analysis of PEEK, African land giant snail shell powder, and sea snail shell powder revealed distinct characteristics for each material, providing valuable insights into their potential for forming hydroxyapatite coatings in bone implant applications.

PEEK exhibited a maximum furrow depth of 0.5527 μm, with a mean depth of 0.1342 μm and a mean density of 4.582 cm/cm^2. These results

indicate relatively shallow furrows and a high density of furrows on the surface of PEEK. The fractal dimension of PEEK was found to be 2.644, revealing a complex and intricate surface morphology (see Fig. 4). The ISO 25178 roughness parameters, such as Sq, Sku, Spk, Svk, Smrk1, Smrk2, Spq, Svq, and Smq, further characterised PEEK's surface roughness and topography. Additionally, the step height calculations revealed a projected area of 274.5 mm^2, a mean void thickness of 0.001259 μm, and a mean material thickness of 0.2487 μm. These measurements provide insights into the surface topography and thickness distribution of PEEK.

African land giant snail shell powder displayed a maximum furrow depth of 84.69 nm, with a mean depth of 24.71 nm and a mean density of 3.816 cm/cm^2. The fractal dimension of giant snail shell powder was 2.376, suggesting a less complex surface morphology than PEEK as presented in Fig. 5. The ISO 25178 roughness parameters, including Sk, Spk, Svk, Smrk1, and Smrk2, further characterised the surface properties. The morphological envelope analysis revealed a height difference of −60.57 nm between cursors and a high material ratio (Smr) of 95.00 %, indicating a substantial proportion of material compared to voids.

Sea snail shell powder demonstrated a maximum furrow depth of 67.75 nm, with a mean depth of 7.185 nm and a mean density of 3.816 cm/cm^2. The fractal dimension of sea snail shell powder was also 2.376, suggesting a similar surface complexity as African land giant snail shell powder. The ISO 25178 roughness parameters, along with morphological envelope analysis, provided insights into the surface properties, including core height (Sk), reduced peak height (Spk), reduced pit depth (Svk), and upper and lower bearing areas (Smrk1 and Smrk2). Comparing the results of the three materials, PEEK exhibited the shallowest furrows and the highest density of furrows. African land giant snail shell powder had deeper furrows, while sea snail shell powder showed intermediate furrow depth. These variations in furrow depth and density are important considerations for forming hydroxyapatite coatings, as they influence the coating's uniformity and stability It was revealed that Fig. 5(a) shows step height calculations of z-difference of 0.1464μm while (b) illustrates SEM intensity surface image whereas (c) presents cell pattern on the scaffold Filled point of KL transformed and Fig. 5(d) revealed morphological envelopes fractal analysis of dimension 2.64.

The materials' surface characteristics, roughness parameters, and morphological properties play a significant role in their biocompatibility and osteoconductivity. With its shallow furrows and high density, the PEEK may provide a favourable substrate for hydroxyapatite coating formation. Despite its deeper furrows, African land giant snail shell powder presents a potential for hydroxyapatite transformation due to its high material ratio. Sea snail shell powder exhibits intermediate furrow depth and density, requiring further investigation to optimise its

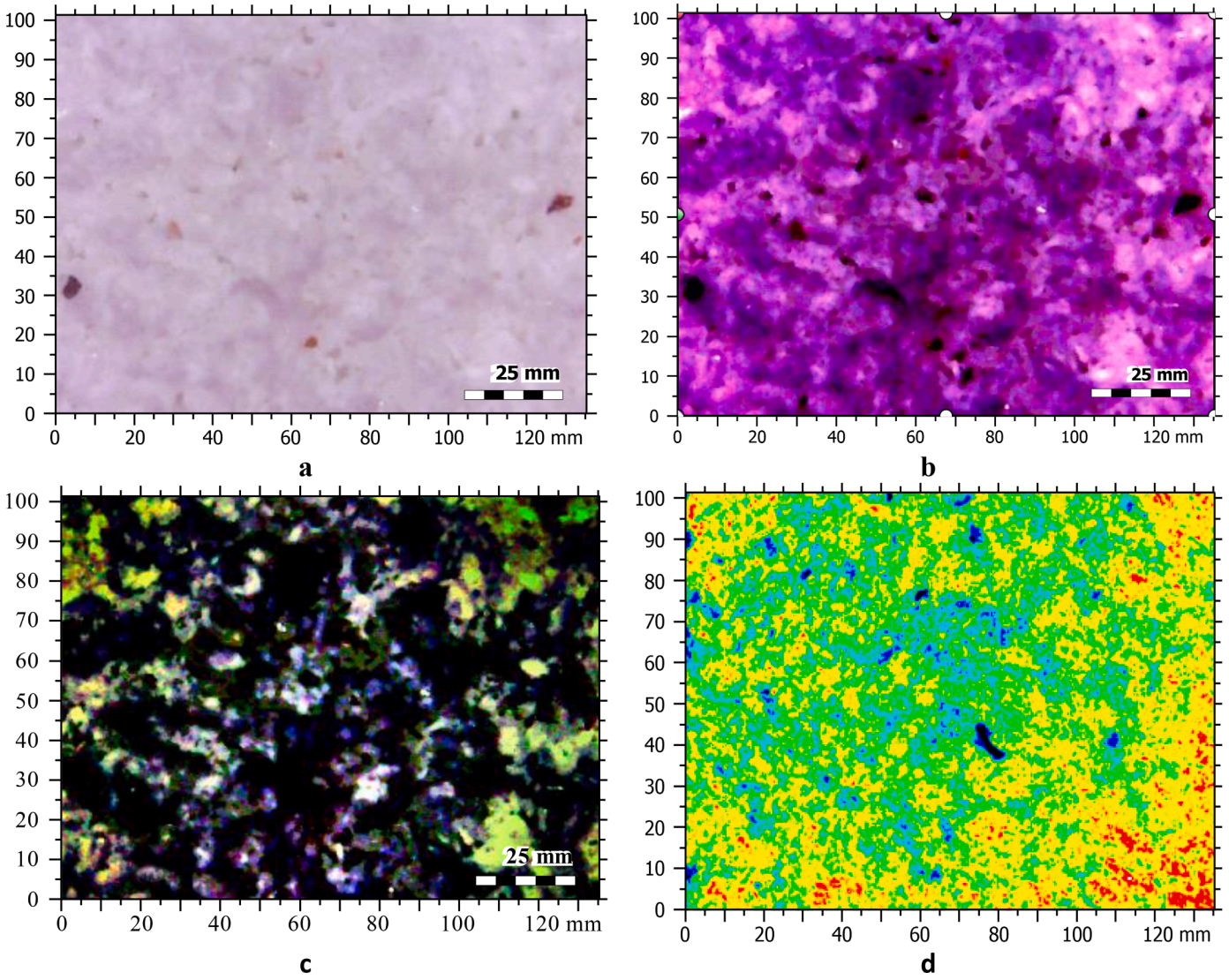

Fig. 4. (a) PEEK/ALGSS/SSS (b) Enhance particle of composite (c) High pass robust Gaussian filter of 285 particle (d) Volume of a hole and peak.

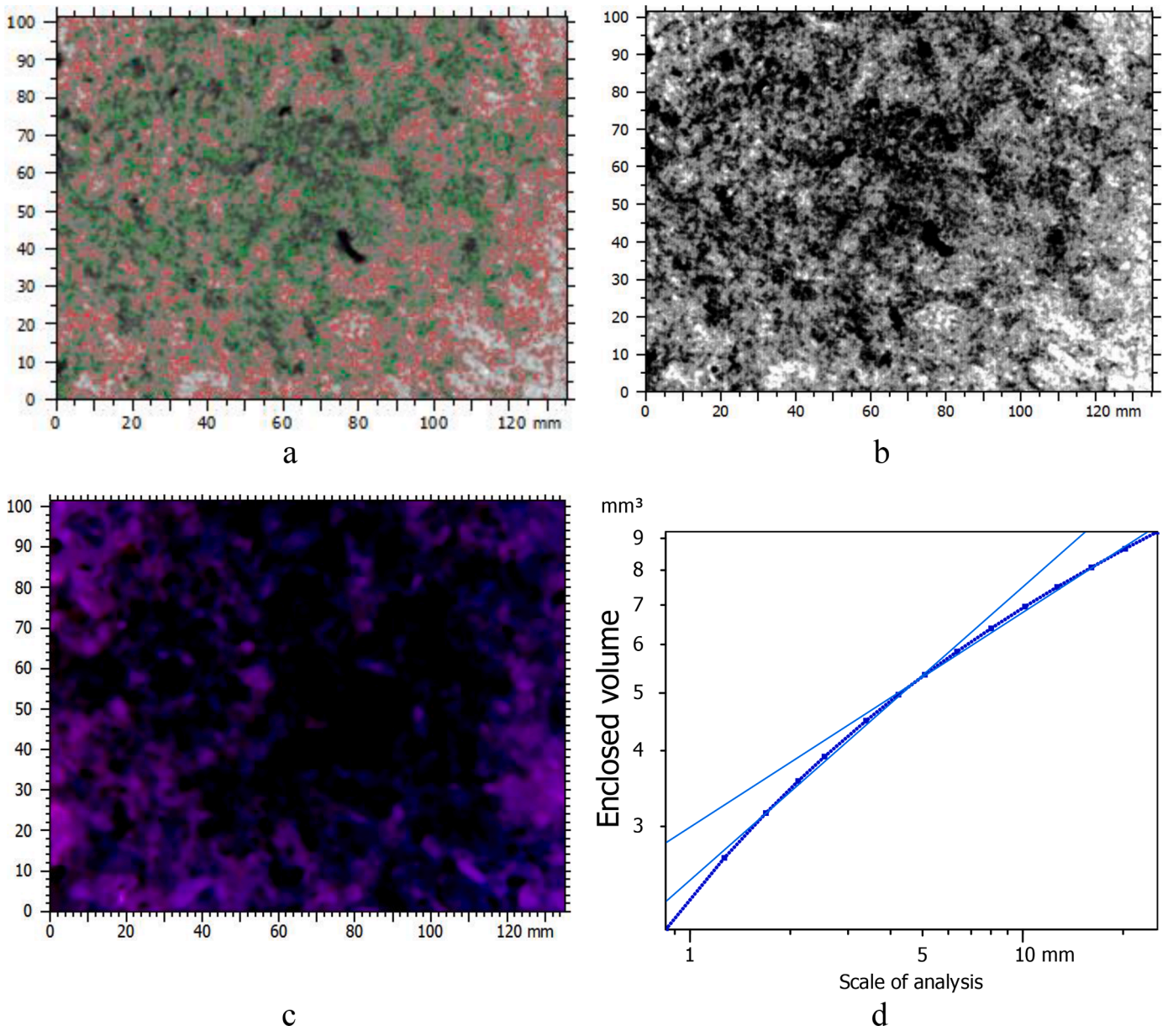

Fig. 5. (a) Step height calculations of z-difference of 0.1464 μm (b) SEM intensity surface image (c) Cell pattern on the scaffold Filled point of KL transformed (d) Morphological envelopes Fractal analysis of dimension 2.64.

potential as a precursor for hydroxyapatite coatings. These results demonstrate the importance of understanding the nanostructure properties of materials intended for bone implant applications. The surface morphology, roughness, and topography significantly impact the interaction between the implant material and the surrounding biological medium.

4.1. Discussion

The analysis of the nanostructures revealed distinctive properties of the materials and the profiles are presented in Fig. 6. The PEEK demonstrated relatively shallow furrows and a high density of furrows, indicating its potential for bone implant applications. The African land giant snail shell powder exhibited deeper furrows and lower density, suggesting challenges in its direct application as a bone implant material. The sea snail shell powder showed intermediate furrow depth and density, offering further optimisation that may be necessary for its utilisation in bone implants. The ISO 25178 parameters and step height calculations provided additional insights into the materials' surface roughness and thickness distribution. The nanostructure analysis of PEEK, African land giant snail shell powder, and sea snail shell powder offers valuable insights into their potential for forming hydroxyapatite coatings in bone implant applications. The results highlight the distinct characteristics of each material, which are crucial factors to consider when designing and developing implant materials with enhanced biocompatibility and osteoconductive [48–50].

PEEK, a high-performance polymer, is known for its excellent mechanical properties and biocompatibility. The shallow furrows and high density of furrows observed in PEEK indicate a relatively smooth surface (see Fig. 7), which can be advantageous for hydroxyapatite coating formation. The surface roughness parameters obtained from ISO 25178 analysis in Fig. 8 provide further details about the topography and roughness of PEEK. The fractal dimension 2.644 suggests a complex surface morphology, which may contribute to increased surface area and improved cell adhesion. These characteristics make PEEK a promising material for bone implants, as incorporating hydroxyapatite coatings

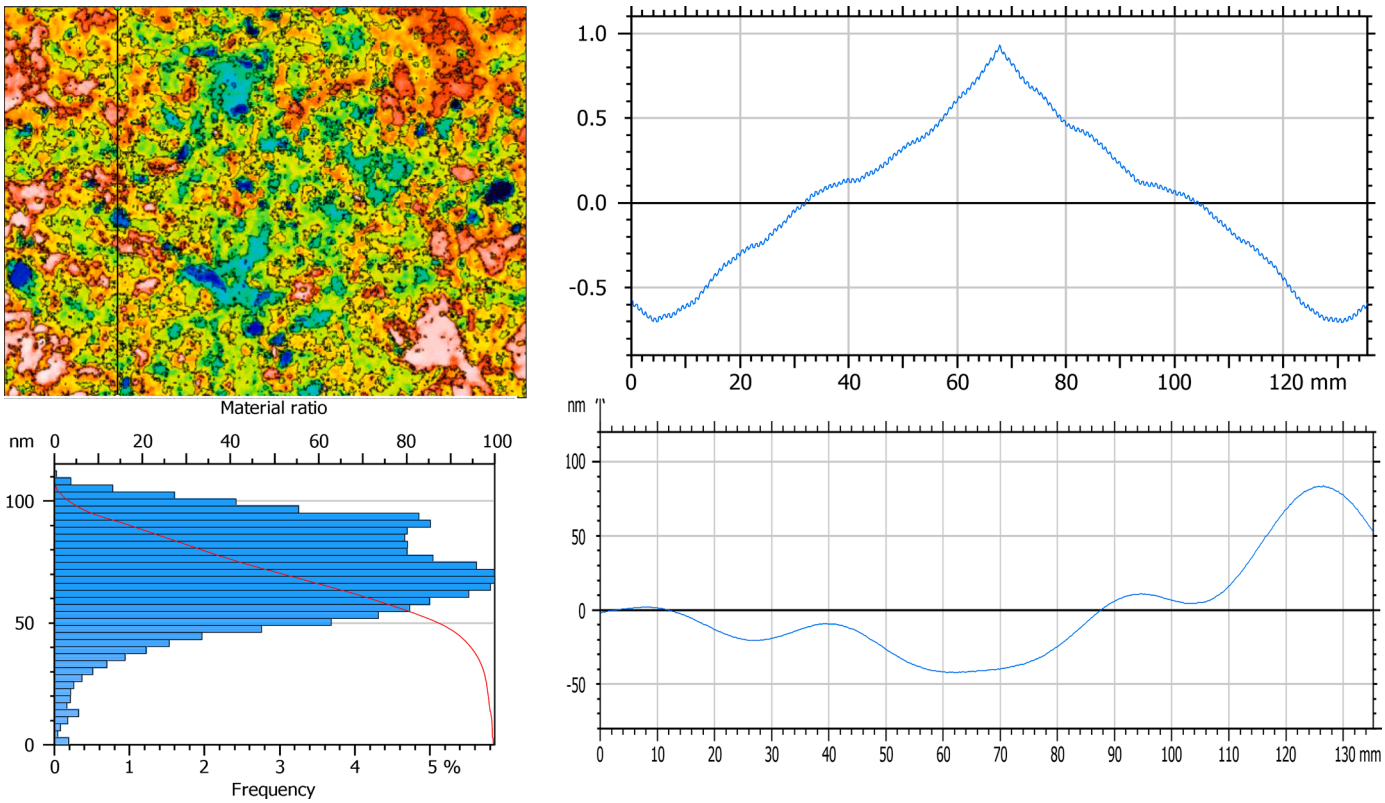

Fig. 6. (a) nanostructure of S-filtere of λs 25 μm (b,d) profile cure of the vertical section of the scaffold (c) Histogram and Abbott curve for material ratio in nanostructure Height difference 0.2926 μm at of points between cursors of 90 %.

can enhance its osteoconductivity and promote osseointegration [67–70]. Despite exhibiting deeper furrows compared to PEEK, giant snail shell powder presents interesting features for hydroxyapatite formation. The high material ratio (Smr) indicates a substantial proportion of material compared to voids, suggesting a favourable environment for hydroxyapatite conversion. The surface roughness parameters and morphological envelope analysis provide a comprehensive understanding of the topography and roughness characteristics of the material. While further optimisation may be required to mitigate the deeper furrows, African land giant snail shell powder's hierarchical structure and calcium carbonate composition offer the potential for hydroxyapatite coating deposition and bone integration [71–74].

Sea snail shell powder demonstrates intermediate furrow depth and density (see Fig. 7), presenting an intriguing nanostructure for bone implant applications. As revealed by the ISO 25178 analysis, the surface properties provide insights into the core height, reduced peak height, reduced pit depth, and bearing areas of the material. These parameters can influence the coating deposition process and the subsequent biological response. Further investigation is necessary to fully understand the potential of sea snail shell powder as a precursor for hydroxyapatite coatings and optimise its nanostructure and surface properties for improved implant integration. The nanostructure analysis conducted in this study highlights the importance of surface characteristics in bone implant materials [75–78]. The specific topography, roughness, and furrow depth can significantly influence the implants' biocompatibility, osseointegration, and long-term performance. Hydroxyapatite coatings enhance these properties by promoting bioactivity and facilitating bone tissue integration. Therefore, tailoring the nanostructure of materials like PEEK, African land giant snail shell powder, and sea snail shell powder is critical to optimising their interaction with the biological environment.

It is important to note that the nanostructure analysis provides a preliminary assessment of the material's potential for hydroxyapatite coating formation. Other factors, such as mechanical properties, degradation behaviour, and biological response, should also be considered in the comprehensive evaluation of these materials for bone implant applications [79–82]. Additionally, the synthesis and fabrication processes in converting the materials into hydroxyapatite coatings require further investigation to determine these approaches' feasibility, scalability, and cost-effectiveness. Future research should develop optimised methods for transforming these nanostructured materials into hydroxyapatite coatings. Techniques such as surface modification, surface functionalisation, and controlled deposition processes can be explored to tailor the nanostructure and improve the bioactivity of the coatings. *In vitro* and *in vivo* studies are also essential to assess the cytocompatibility, tissue integration, and long-term performance of the hydroxyapatite-coated materials.

In conclusion, the nanostructure analysis of PEEK, African land giant snail shell powder, and sea snail shell powder provides valuable insights into their potential for forming hydroxyapatite coatings in bone implant applications. Each material exhibits unique characteristics that can be leveraged for enhanced biocompatibility and osseointegration. Further optimisation of these materials and developing effective coating strategies are necessary to advance their potential as bone implant materials. The findings of this study lay the foundation for future research in the field of nanostructured materials for bone implants, it is an impactful study contributing to the ongoing efforts to improve patient outcomes and quality of life in orthopaedic surgery.

4.2. *Clinical implications*

The distinct nanostructure characteristics of these materials have a direct impact on their interaction with the biological environment. Surface characteristics, roughness, and furrow depth significantly influence the biocompatibility, osseointegration, and long-term performance of bone implants. The incorporation of hydroxyapatite coatings

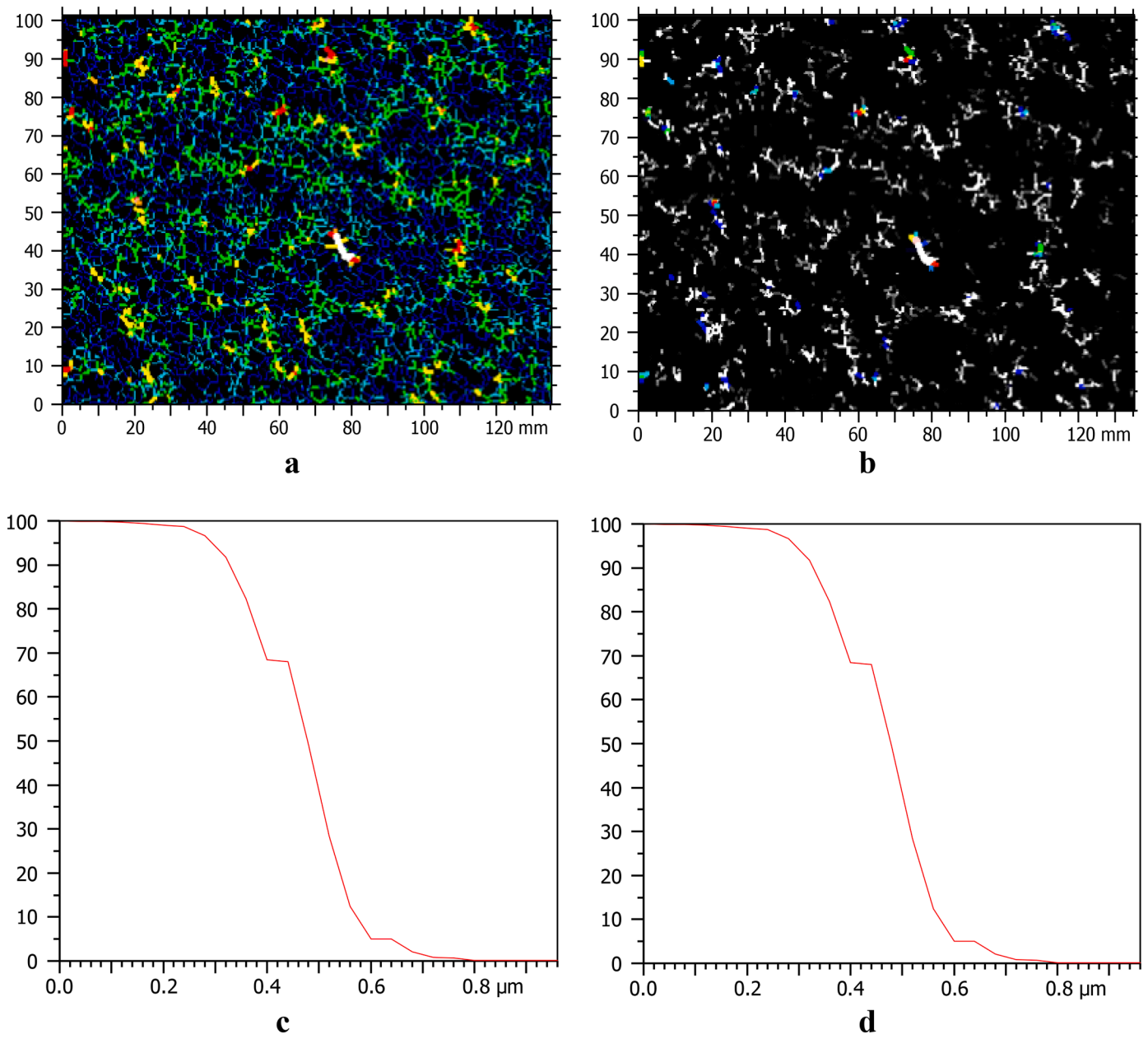

Fig. 7. (a)Furrows particle parameters showing the Maximum depth of furrows of 0.5527 µm, Mean depth of 0.1342 µm and Mean density of 4.582 cm/cm^2 (b) the furrows deeper than the threshold are showing Parameters of Maximum depth of furrows 0.5527 µm at Mean depth of 0.3565 µm Mean density of 0.07749 cm/cm^2 (c) Curve display mode Particle count distribution log curve (d) Area curve.

further enhances these properties by promoting bioactivity and facilitating bone tissue integration.

The findings of this study lay the groundwork for further research in the field of nanostructured materials for bone implants. The unique characteristics of PEEK, African land giant snail shell powder, and sea snail shell powder's nanostructures offer opportunities for the advancement of bone implant materials, contributing to improved patient outcomes and quality of life in orthopedic surgery.

However, it is essential to consider that the nanostructure analysis provides only a preliminary assessment of the materials' potential for hydroxyapatite coating formation. Other factors, such as mechanical properties, degradation behavior, and biological response, must also be taken into account for a comprehensive evaluation of these materials for bone implant applications. *In vitro* and *in vivo* studies will be crucial to assess the cytocompatibility, tissue integration, and long-term performance of the hydroxyapatite-coated materials.

5. Conclusion

In conclusion, the experimental research conducted on the nanostructure analysis of PEEK, giant snail shell powder, and sea snail shell powder for forming hydroxyapatite coatings in bone implant applications provides valuable insights into the suitability of these materials. Each material exhibits unique characteristics that contribute to its potential as a novel and ideal candidate for bone implants. PEEK, a high-performance polymer, offers excellent mechanical properties and biocompatibility. The shallow furrows and high density of furrows observed in PEEK indicate a favourable surface for hydroxyapatite coating formation, enhancing its osteoconductivity and promoting osseointegration. The combination of PEEK's properties and the incorporation of hydroxyapatite coatings present a promising approach to developing advanced bone implants.

Despite its deeper furrows, African land giant snail shell powder

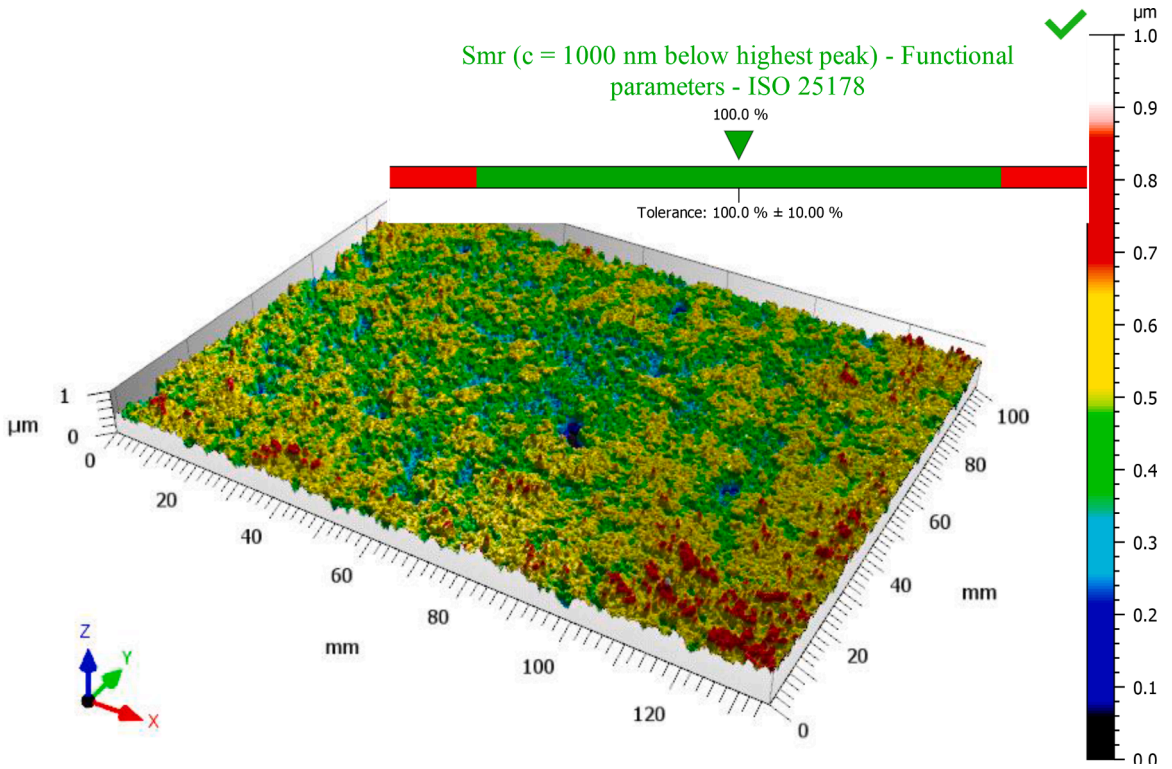

Fig. 8. 3D view of surface KL transformed and functional parameters of ISO 25178.

possesses a hierarchical structure and a high material ratio, making it a compelling precursor for hydroxyapatite formation. The unique nanostructure and composition of big snail shell powder provide an opportunity to develop novel bone implant materials with enhanced bioactivity and improved integration with bone tissue. Sea snail shell powder demonstrates an intermediate furrow depth and density, suggesting its potential for hydroxyapatite coating formation. Further optimisation of its nanostructure and surface properties can unlock its full potential as a precursor for bone implants. Exploring sea snail shell powder as a material for hydroxyapatite coatings offers an innovative avenue for developing biomimetic and bioactive implant surfaces.

The novelty of this research lies in the comprehensive analysis of the nanostructure properties of these materials, which sheds light on their potential for bone implant applications. By investigating the surface roughness, furrow depth, density, and other relevant parameters, this study contributes to understanding the materials' interactions with the biological environment and their ability to support bone regeneration and integration. The findings of this research emphasise the importance of nanostructure characterisation in the design and development of bone implants. The tailored nanostructure of PEEK, giant snail shell powder, and sea snail shell powder can significantly influence their biocompatibility, osseointegration, and long-term performance. By optimising the materials and coating strategies, the field of bone implantology can benefit from the enhanced functionality and improved clinical outcomes offered by these nanostructured materials.

In conclusion, the findings of this study lay the groundwork for further research in the field of nanostructured materials for bone implants. The unique characteristics of PEEK, African land giant snail shell powder, and sea snail shell powder's nanostructures offer opportunities for the advancement of bone implant materials, contributing to improved patient outcomes and quality of life in orthopedic surgery. The research objective of the paper was to analyze the nanostructure of three materials (PEEK, African land giant snail shell powder, and sea snail shell powder) for potential hydroxyapatite coatings in bone implants. The study evaluated surface characteristics, furrow depth, and density to assess their suitability as coating substrates. The specific materials studied were Polyether Ether Ketone (PEEK), African Giant Snail Shell (ALGSS) Powder, and Sea Snail Shell (SSS) Powder. This analysis offers insights into their potential as bone implant materials for hydroxyapatite coatings, contributing to improved biocompatibility and clinical outcomes in bone implantology.

Finally, the findings of this study lay the groundwork for further research in the field of nanostructured materials for bone implants. The unique characteristics of PEEK, African land giant snail shell powder, and sea snail shell powder's nanostructures offer opportunities for the advancement of bone implant materials, contributing to improved patient outcomes and quality of life in orthopedic surgery.

5.1. *Future research recommendations*

Future research should focus on developing optimized methods for transforming these nanostructured materials into hydroxyapatite coatings, exploring techniques like surface modification and controlled deposition processes. Another future research should focus on further optimising the nanostructure of these materials and exploring advanced fabrication techniques to improve their bioactivity, mechanical properties, and overall performance. Additionally, *in vitro* and *in vivo* studies are necessary to evaluate these materials' cytocompatibility, tissue integration, and long-term efficacy in bone implant applications. In conclusion, this research demonstrates the potential of PEEK, African land giant snail shell powder, and sea snail shell powder for forming hydroxyapatite coatings in bone implant applications. These materials' unique nanostructure and surface properties offer exciting prospects for developing next-generation bone implants with enhanced biocompatibility and improved clinical outcomes. Further research and development in this field can contribute to advancements in orthopaedic surgery and positively impact the lives of patients needing bone reconstruction or replacement.

Ethical approval

This study does not contain any studies with human or animal subjects performed by any of the authors.

Compliance with ethics guidelines

None.

Ethical statement

The authors declare no ethical issue; the study was conducted in complete agreement with ethical standards. Also, the manuscript is neither under review nor published elsewhere.

CRediT authorship contribution statement

Agbor A. Esoso: Data curation, Conceptualization, Formal analysis, Methodology, Investigation, Writing – original draft. **Tien-Chien Jen:** Formal analysis, Methodology, Writing – review & editing. **Omolayo M. Ikumapayi:** Formal analysis, Software, Writing – review & editing. **Bankole I. Oladapo:** Formal analysis, Software, Methodology, Writing – review & editing. **Esther T. Akinlabi:** Formal analysis, Software, Methodology, Writing – review & editing.

Declaration of Competing Interest

The authors declare that they have no known competing for financial interests or personal relationships that could have appeared to influence the work reported in this paper.

Acknowledgment

None.

References

[1] W. Lai, Y. Wang, H. Fu, J. He, Hydroxyapatite/polyetheretherketone nanocomposites for selective laser sintering: thermal and mechanical performances, E-Polymers 20 (2020) 542–549, https://doi.org/10.1515/epoly-2020-0057.

[2] Q. Hu, Y. Wang, S. Liu, Q. Liu, H. Zhang, 3D printed polyetheretherketone bone tissue substitute modified *via* amoxicillin-laden hydroxyapatite nanocoating, J. Mater. Sci. 57 (2022) 18601–18614, https://doi.org/10.1007/S10853-022-07782-9.

[3] B.I. Oladapo, S.A. Zahedi, Improving bioactivity and strength of PEEK composite polymer for bone application, Mater. Chem. Phys. 266 (2021), 124485, https://doi.org/10.1016/j.matchemphys.2021.124485.

[4] B.I. Oladapo, S.A. Zahedi, S.O. Ismail, Mechanical performances of hip implant design and fabrication with PEEK composite, Polymer 227 (2021), 123865, https://doi.org/10.1016/J.POLYMER.2021.123865 (Guildf).

[5] M. Tlotleng, E. Akinlabi, M. Shukla, S. Pityana, Microstructures, Hardness and Bioactivity of Hydroxyapatite Coatings Deposited by Direct Laser Melting Process, J. Mater. Sci. Eng. C 43 (2014) 189–198.

[6] B.I. Oladapo, A.V. Adebiyi, E. Ifeoluwa Elemure, Microstructural 4D printing investigation of ultra-sonication biocomposite polymer, J. King Saud Univ. Eng. Sci. 33 (2021) 54–60, https://doi.org/10.1016/j.jksues.2019.12.002.

[7] B.I. Oladapo, S.A. Zahedi, A.O.M. Adeoye, 3D printing of bone scaffolds with hybrid biomaterials, Compos. B Eng. 158 (2019) 428–436, https://doi.org/10.1016/J.COMPOSITESB.2018.09.065.

[8] B.I. Oladapo, S.Z. Abolfazl, V.A. Balogun, S.O. Ismail, Y.A. Samad, Overview of additive manufacturing of biopolymer composites, in: D. Brabazon (Ed.), Encyclopedia of Materials: Composites, 1st ed., Elsevier, 2021.

[9] B. Oladapo, A. Zahedi, S. Ismail, W. Fernando, O. Ikumapayi, 3D-printed biomimetic bone implant polymeric composite scaffolds, Int. J. Adv. Manuf. Technol. 126 (2023) 4259–4267, https://doi.org/10.1007/S00170-023-11344-X/FIGURES/5.

[10] B.I. Oladapo, S.O. Ismail, O.M. Ikumapayi, P.G. Karagiannidis, Impact of rGO-coated PEEK and lattice on bone implant, Colloids Surf. B Biointerfaces 216 (2022), 112583, https://doi.org/10.1016/J.COLSURFB.2022.112583.

[11] B.I. Oladapo, S.A. Zahedi, S.O. Ismail, F.T. Omigbodun, 3D printing of PEEK and its composite to increase biointerfaces as a biomedical material- A review, Colloids Surf. B Biointerfaces 203 (2021), 111726, https://doi.org/10.1016/J.COLSURFB.2021.111726.

[12] C. Koski, B. Onuike, A. Bandyopadhyay, S. Bose, Starch-hydroxyapatite composite bone scaffold fabrication utilising a slurry extrusion-based solid freeform fabricator, Addit. Manuf. 24 (2018) 47–59, https://doi.org/10.1016/j.addma.2018.08.030.

[13] C. Prakash, G. Singh, S. Singh, W.L. Linda, H.Y. Zheng, S. Ramakrishna, et al., Mechanical reliability and *in vitro* bioactivity of 3D-printed porous polylactic acid-hydroxyapatite scaffold, J. Mater. Eng. Perform. 30 (2021) 4946–4956, https://doi.org/10.1007/S11665-021-05566-X.

[14] C.S. Wu, S.S. Wang, D.Y. Wu, W.L. Shih, Novel composite 3D-printed filament made from fish scale-derived hydroxyapatite, eggshell and polylactic acid *via* a fused fabrication approach, Addit. Manuf. 46 (2021), https://doi.org/10.1016/j.addma.2021.102169.

[15] B.I. Oladapo, S.A. Zahedi, S.O. Ismail, D.B. Olawade, Recent advances in biopolymeric composite materials: future sustainability of bone-implant, Renew. Sustain. Energy Rev. 150 (2021), 111505, https://doi.org/10.1016/J.RSER.2021.111505.

[16] B.I. Oladapo, S. Abolfazl Zahedi, F. Vahidnia, O.M. Ikumapayi, M.U Farooq, Three-dimensional finite element analysis of a porcelain crowned tooth, Beni-Suef Univ. J. Basic Appl. Sci. 7 (2018) 461–464, https://doi.org/10.1016/j.bjbas.2018.04.002.

[17] B.I. Oladapo, J.F. Kayode, J.O. Akinyoola, O.M. Ikumapayi, Shape memory polymer review for flexible artificial intelligence materials of biomedical, Mater. Chem. Phys. 293 (2023), https://doi.org/10.1016/J.MATCHEMPHYS.2022.126930.

[18] B.I. Oladapo, S.O. Ismail, M. Zahedi, A. Khan, H. Usman, 3D printing and morphological characterisation of polymeric composite scaffolds, Eng. Struct. 216 (2020), 110752, https://doi.org/10.1016/j.engstruct.2020.110752.

[19] B.I. Oladapo, S.A. Zahedi, S.O. Ismail, D.B. Olawade, Recent advances in biopolymeric composite materials: future sustainability of bone-implant, Renew. Sustain. Energy Rev. 150 (2021), 111505, https://doi.org/10.1016/j.rser.2021.111505.

[20] M. Tlotleng, E. Akinlabi, M. Shukla, Mechanical and Microstructural Evaluation of Laser Assisted Cold Sprayed Bio-ceramic Coatings: Potential Use for Biomedical Applications, J. Therm. Spray Technol. 24 (2015) 423–435.

[21] B.I. Oladapo, S.O. Ismail, T.D. Afolalu, D.B. Olawade, M. Zahedi, Review on 3D printing: fight against COVID-19, Mater. Chem. Phys. 258 (2021), 123943, https://doi.org/10.1016/j.matchemphys.2020.123943.

[22] S.I. Saidu, N. Orimabuyaku, B.A. Ademola, O.V. Amadi, D. Olawade, B.I. Oladapo, et al., Strengthening medical outreach: enhancing healthcare access in developing countries, Int. J. Sci. Res. Arch. 8 (2023) 552–558, https://doi.org/10.30574/IJSRA.2023.8.2.0296.

[23] M. Pizzorni, E. Lertora, A. Parmiggiani, Adhesive bonding of 3D-printed short- and continuous-carbon-fiber composites: an experimental analysis of design methods to improve joint strength, Compos. B Eng. 230 (2022), https://doi.org/10.1016/j.compositesb.2021.109539.

[24] Z. Hou, X. Tian, J. Zhang, D. Li, 3D printed continuous fibre reinforced composite corrugated structure, Compos. Struct. 184 (2018) 1005–1010, https://doi.org/10.1016/j.compstruct.2017.10.080.

[25] Z. Hashin, Analysis of composite materials: a survey, J. Appl. Mech. Trans. ASME 50 (1983) 481–505, https://doi.org/10.1115/1.3167081.

[26] M. Nasr Azadani, A. Zahedi, O.K. Bowoto, B.I. Oladapo, A review of current challenges and prospects of magnesium and its alloy for bone implant applications, Prog. Biomater. 11 (1) (2022) 1–26, https://doi.org/10.1007/S40204-022-00182-X, 2022;11.

[27] B.I. Oladapo, S.A. Zahedi, S.O. Ismail, F.T. Omigbodun, O.K. Bowoto, M. A. Olawumi, et al., 3D printing of PEEK–cHAp scaffold for medical bone implant, Bio-Des Manuf. 4 (2021) 44–59, https://doi.org/10.1007/s42242-020-00098-0.

[28] B.I. Oladapo, S.O. Ismail, O.K. Bowoto, F.T. Omigbodun, M.A. Olawumi, M. A. Muhammad, Lattice design and 3D-printing of PEEK with Ca10(OH)(PO4)3 and *in-vitro* bio-composite for bone implant, Int. J. Biol. Macromol. 165 (2020) 50–62, https://doi.org/10.1016/j.ijbiomac.2020.09.175.

[29] B.I. Oladapo, S.O. Ismail, A.V. Adebiyi, F.T. Omigbodun, M.A. Olawumi, D. B. Olawade, Nanostructural interface and strength of polymer composite scaffolds applied to intervertebral bone, Colloids Surf. A Physicochem. Eng. Asp. 627 (2021), 127190, https://doi.org/10.1016/J.COLSURFA.2021.127190.

[30] Y.K. Jimah, R.O. Okojie, S.O. Akinlabi, A.R. Olawaled, J.F. Kayode, Aligning humanitarian outreach with united nations sustainable development goals, World J. Adv. Res. Rev. 18 (02) (2023) 051–056, https://doi.org/10.30574/wjarr.2023.18.2.0642.

[31] B.I. Oladapo, J.F. Kayode, P. Karagiannidis, N. Naveed, H. Mehrabi, K. O. Ogundipe, Polymeric composites of cubic-octahedron and gyroid lattice for biomimetic dental implants, Mater. Chem. Phys. 289 (2022), https://doi.org/10.1016/J.MATCHEMPHYS.2022.126454.

[32] B.I. Oladapo, I.A. Daniyan, O.M. Ikumapayi, O.B. Malachi, I.O. Malachi, Microanalysis of hybrid characterisation of PLA/cHA polymer scaffolds for bone regeneration, Polym. Test. 83 (2020), 106341, https://doi.org/10.1016/j.polymertesting.2020.106341.

[33] O.M. Ikumapayi, T.S. Ogedengbe, A.T. Ogundipe, E.S. Nnochiri, B.A. Obende, S. A. Afolalu. Ceramics matrix composites for biomedical applications - a review. *Materials Today: Proceedings*, 2023. https://doi.org/10.1016/j.matpr.2023.08.168.

[34] B.I. Oladapo, O.B. Obisesan, B. Oluwole, V.A. Adebiyi, H. Usman, A. Khan, Mechanical characterisation of a polymeric scaffold for bone implant, J. Mater. Sci. 55 (2020) 9057–9069, https://doi.org/10.1007/s10853-020-04638-y.

[35] A.B. Olorunsola, O.M. Ikumapayi, B.I. Oladapo, A.O. Alimi, A.O.M. Adeoye, Temporal variation of exposure from radio-frequency electromagnetic fields

around mobile communication base stations, Sci. Afr. 12 (2021) e00724, https://doi.org/10.1016/J.SCIAF.2021.E00724.
[36] U. Fasel, D. Keidel, L. Baumann, G. Cavolina, M. Eichenhofer, P. Ermanni, Composite additive manufacturing of morphing aerospace structures, Manuf. Lett. 23 (2020) 85–88, https://doi.org/10.1016/j.mfglet.2019.12.004.
[37] C. Quan, B. Han, Z. Hou, Q. Zhang, X. Tian, T.J. Lu, 3d printed continuous fiber reinforced composite auxetic honeycomb structures, Compos. B Eng. 187 (2020), https://doi.org/10.1016/j.compositesb.2020.107858.
[38] S.J. Pickering, Recycling technologies for thermoset composite materials-current status, Compos. Part A Appl. Sci. Manuf. 37 (2006) 1206–1215, https://doi.org/10.1016/j.compositesa.2005.05.030.
[39] M. Tlotleng, E.T. Akinlabi, M. Shukla (Eds.), Pityana. Application of Laser Assisted Cold Spraying Process for Materials Deposition. In: Surface Engineering Techniques and Applications: Research Advancements edited by Loredana Santo and J. Paulo Davim published by IGI publishing, USA, 2014, ISBN 9781466651418.
[40] J. Xu, Y. Ling, X. Zheng, Forensic detection of Gaussian low-pass filtering in digital images, in: Proceedings of the 2015 8th International Congress on Image and Signal Processing (CISP), IEEE, 2015, pp. 819–823.
[41] K.C. McPhee, C. Denk, Z. AlRekabi, A. Rauscher, Bilateral filtering of magnetic resonance phase images, Magn. Reson. Imaging 29 (7) (2011) 1023–1029.
[42] X. Chen, J. Yang, Q. Wu, J. Zhao, X. He, Directional high-pass filter for blurry image analysis, Signal Process. Image Commun. 27 (7) (2012) 760–771.
[43] S. Lou, X. Jiang, P.J. Scott, Correlating motif analysis and morphological filters for surface texture analysis, Measurement 46 (2) (2013) 993–1001.
[44] L.L. Graham, R. Harris, W. Villiger, T.J. Beveridge, Freeze-substitution of gram-negative eubacteria: general cell morphology and envelope profiles, J. Bacteriol. 173 (5) (1991) 1623–1633.
[45] J.C. Nunes, Y. Bouaoune, E. Delechelle, O. Niang, P. Bunel, Image analysis by bidimensional empirical mode decomposition, Image Vis. Comput. 21 (12) (2003) 1019–1026.
[46] ISO 25178-2:2021Geometrical product specifications (GPS) — Surface texture: Areal — Part 2: Terms, definitions and surface texture parameters https://www.iso.org/standard/74591.html.
[47] ISO 4287:1997Geometrical Product Specifications (GPS) — Surface texture: Profile method — Terms, definitions and surface texture parameters. https://www.iso.org/standard/10132.html.
[48] A. Logins, T. Torims, The influence of high-speed milling strategies on 3D surface roughness parameters, Proc. Eng. 100 (2015) 1253–1261.
[49] N. Bulaha, Analysis of service properties of cylindrically ground surfaces, using standard ISO 25178-2: 2012 surface texture parameters, in: Environment, Technologies, Resources. Proceedings of the International Scientific and Practical Conference 1, 2015, pp. 16–21.
[50] F. Marinello, A. Pezzuolo, Application of ISO 25178 standard for multiscale 3D parametric assessment of surface topographies, IOP Conf. Ser. Earth Environ. Sci. 275 (1) (2019), 012011. IOP Publishing.
[51] J. Bennett, Measuring UV curing parameters of commercial photopolymers used in additive manufacturing, Addit. Manuf. 18 (2017) 203–212.
[52] A. Mohan, S. Poobal, Crack detection using image processing: a critical review and analysis, Alex. Eng. J. 57 (2) (2018) 787–798.
[53] A. A. B. Abadi, S. Tahcfulloh. Digital Image Processing for Height Measurement Application Based on Python OpenCV and Regression Analysis. Politeknik Negeri Padang. 6,(4) (2022). 763–770. https://doi.org/10.30630/joiv.6.4.1013.
[54] K. Zidek, J. Piteľ, A. Hošovský, Design of adjustable smart vision system based on artificial muscle actuators, MM Sci. J. 2016 (2016) 947–951, https://doi.org/10.17973/MMSJ.2016_09_201635.
[55] S. Kesić, S.Z. Spasić, Application of Higuchi's fractal dimension from basic to clinical neurophysiology: a review, Comput. Methods Programs Biomed. 133 (2016) 55–70.
[56] S. Zahid, R. Dolz-Marco, K.B. Freund, C. Balaratnasingam, K. Dansingani, F. Gilani, N. Mehta, E. Young, M.R. Klifto, B. Chae, L.A. Yannuzzi, Fractal dimensional analysis of optical coherence tomography angiography in eyes with diabetic retinopathy, Invest. Ophthalmol. Vis. Sci. 57 (11) (2016) 4940–4947.
[57] S. Siddiqui, M.S. Khan, K. Ferens, W. Kinsner, Detecting advanced persistent threats using fractal dimension based machine learning classification, in: Proceedings of the 2016 ACM on International Workshop on Security and Privacy Analytics, 2016, pp. 64–69.
[58] S. Jin, J. Zhang, S. Han, Fractal analysis of relation between strength and pore structure of hardened mortar, Constr. Build. Mater. 135 (2017) 1–7.
[59] G. Turnbull, J. Clarke, F. Picard, P. Riches, L. Jia, F. Han, et al., 3D bioactive composite scaffolds for bone tissue engineering, Bioact. Mater. 3 (2018) 278–314, https://doi.org/10.1016/j.bioactmat.2017.10.001.
[60] H. Ghiasi, K. Fayazbakhsh, D. Pasini, L. Lessard, Optimum stacking sequence design of composite materials part II: variable stiffness design, Compos. Struct. 93 (2010) 1–13, https://doi.org/10.1016/j.compstruct.2010.06.001.
[61] A.R. Toibah, I. Sopyan, M. Hamdi, S. Ramesh, Development of Magnesium-Doped Biphasic Calcium Phosphatethrough Sol-Gel Method, International Islamic University Malaysia /Department of Manufacturing and Materials Engineering, Faculty of Engineering, 2008. Kuala Lumpur, Malaysia.
[62] O. Gunduz, Y.M. Sahin, S. Agathopoulos, B. Ben-Nissan, A New Method for Fabrication of Nanohydroxyapatite and TCP from the Sea Snail Cerithium vulgatum, J. Nanomater. (2014) 1–6, https://doi.org/10.1155/2014/382861.
[63] Yazdani B., Chen B., Benedetti L., Davies R., Ghita O., Zhu Y. 2018., A new method to prepare composite powders customized for high temperature laser sintering, College of Engineering, Mathematics and Physical Sciences, University of Exeter, Exeter, EX4 4QF, UK.
[64] S. Pokhrel, Hydroxyapatite: Preparation, Properties and Its Biomedical Applications, Adv. Chem. Eng. 8 (2018) 225–240, https://doi.org/10.4236/aces.2018.84016.
[65] U. Vijayalakshmi, S. Rajeswari, Influence of process parameters on the sol–gel synthesis of nano hydroxyapatite using various phosphorus precursors, J. Sol-Gel Sci. Technol. 63 (2012) 45–55, https://doi.org/10.1007/s10971-012-2762-2.
[66] S. Rujitanapanich, P. Kumpapan, P. Wanjanoi, Synthesis of hydroxyapatite from oyster shell via precipitation, Energy Procedia 56 (2014) 112–117, https://doi.org/10.1016/j.egypro.2014.07.138.
[67] M.C.S. Ribeiro, A. Fiúza, A. Ferreira, L. Dinis M de, A.C.M. Castro, J.P. Meixedo, et al., Recycling approach towards sustainability advance of composite materials' industry, Recycling 1 (2016) 178–193, https://doi.org/10.3390/RECYCLING1010178.
[68] P. Cheng, Y. Peng, S. Li, Y. Rao, A. Le Duigou, K. Wang, et al., 3D printed continuous fiber reinforced composite lightweight structures: a review and outlook, Compos. B Eng. 250 (2023), 110450, https://doi.org/10.1016/J.COMPOSITESB.2022.110450.
[69] T. Tamagawa, Y. Mori, S. Minakuchi, Consolidation mechanism of composite corners cured on convex and concave tools, Compos. Part A Appl. Sci. Manuf. 169 (2023), https://doi.org/10.1016/j.compositesa.2023.107500.
[70] Y. Wang, G. Zhang, H. Ren, G. Liu, Y. Xiong, Fabrication strategy for joints in 3D printed continuous fiber reinforced composite lattice structures, Compos. Commun. 30 (2022), https://doi.org/10.1016/j.coco.2022.101080.
[71] M.C.S. Ribeiro, A.C. Meira-Castro, F.G. Silva, J. Santos, J.P. Meixedo, A. Fiúza, et al., Re-use assessment of thermoset composite wastes as aggregate and filler replacement for concrete-polymer composite materials: a case study regarding GFRP pultrusion wastes, Resour. Conserv. Recycl. 104 (2015) 417–426, https://doi.org/10.1016/j.resconrec.2013.10.001.
[72] B. Shi, Y. Shang, P. Zhang, A.P. Cuadros, J. Qu, B. Sun, et al., Dynamic capillary-driven additive manufacturing of continuous carbon fiber composite, Matter 2 (2020) 1594–1604, https://doi.org/10.1016/j.matt.2020.04.010.
[73] Y. Chen, L. Ye, Topological design for 3D-printing of carbon fibre reinforced composite structural parts, Compos. Sci. Technol. 204 (2021), https://doi.org/10.1016/j.compscitech.2020.108644.
[74] C. Zeng, L. Liu, W. Bian, J. Leng, Y. Liu, Temperature-dependent mechanical response of 4D printed composite lattice structures reinforced by continuous fiber, Compos. Struct. 280 (2022), https://doi.org/10.1016/j.compstruct.2021.114952.
[75] Y. Zhang, J. Qiao, G. Zhang, Y. Li, L. Li, Prediction of deformation and failure behavior of continuous fiber reinforced composite fabricated by additive manufacturing, Compos. Struct. 265 (2021), https://doi.org/10.1016/j.compstruct.2021.113738.
[76] K. Sugiyama, R. Matsuzaki, M. Ueda, A. Todoroki, Y. Hirano, 3D printing of composite sandwich structures using continuous carbon fiber and fiber tension, Compos. Part A Appl. Sci. Manuf. 113 (2018) 114–121, https://doi.org/10.1016/j.compositesa.2018.07.029.
[77] S. Job, Recycling composites commercially, Reinf. Plast. 58 (2014) 32–34, https://doi.org/10.1016/S0034-3617(14)70213-9.
[78] A.E. Krauklis, C.W. Karl, A.I. Gagani, J.K. Jørgensen, Composite material recycling technology—State-of-the-art and sustainable development for the 2020s, J. Compos. Sci. 5 (2021), https://doi.org/10.3390/JCS5010028.
[79] N. Li, G. Link, T. Wang, V. Ramopoulos, D. Neumaier, J. Hofele, et al., Path-designed 3D printing for topological optimised continuous carbon fibre reinforced composite structures, Compos. B Eng. 182 (2020), https://doi.org/10.1016/j.compositesb.2019.107612.
[80] J. Lee, D. Kim, T. Nomura, E.M. Dede, J. Yoo, Topology optimisation for continuous and discrete orientation design of functionally graded fiber-reinforced composite structures, Compos. Struct. 201 (2018) 217–233, https://doi.org/10.1016/j.compstruct.2018.06.020.
[81] M. Chen, H. Zhong, L. Chen, Y. Zhang, M. Zhang, Engineering properties and sustainability assessment of recycled fibre reinforced rubberised cementitious composite, J. Clean. Prod. 278 (2021), https://doi.org/10.1016/j.jclepro.2020.123996.
[82] P. Zhuo, S. Li, I.A. Ashcroft, A.I. Jones, Continuous fibre composite 3D printing with pultruded carbon/PA6 commingled fibres: processing and mechanical properties, Compos. Sci. Technol. 221 (2022), https://doi.org/10.1016/j.compscitech.2022.109341.